

TOOLBOX

Size, organization, and dynamics of soluble SQSTM1 and LC3-SQSTM1 complexes in living cells

Lewis J. Kraft^{a,*}, Jacob Dowler^b, Pallavi Manral^b, and Anne K. Kenworthy^{a,b,c}

^aChemical and Physical Biology Program, Vanderbilt University Medical Center, Nashville, TN, USA; ^bDepartment of Molecular Physiology and Biophysics, Vanderbilt University Medical Center, Nashville, TN, USA; ^cDepartment of Cell and Developmental Biology, Vanderbilt University Medical Center, Nashville, TN, USA

ABSTRACT

Selective macroautophagy/autophagy—with the help of molecular receptors—captures cargo for lysosomal degradation. Among the best-studied molecular receptors is SQSTM1/p62, a homo-oligomeric ubiquitin binding protein, which binds to both cargo and MAP1LC3B/LC3, a protein important for autophagosome biogenesis. Although the mechanisms underlying interaction of LC3 and SQSTM1 have been extensively studied, very little is known about the size or organization of soluble complexes formed between SQSTM1 and LC3 prior to phagophore (the autophagosome precursor) binding in live cells at the molecular level. To address this question, in the current study we use a combination of 2 microscopy-based approaches, FRET microscopy and confocal FRAP, to study the nanoscale properties of soluble SQSTM1 complexes and SQSTM1-LC3 complexes in living HeLa cells. We find that, independent of puncta, SQSTM1 oligomerizes to form very slowly diffusing complexes that contain multiple copies of SQSTM1 within FRET proximity of one another. Furthermore, we show that the interactions of soluble pools of LC3 and SQSTM1 can be readily detected by both FRAP and FRET. Finally, we uncover unexpected roles of SQSTM1's PB1 domain, a region of the protein involved in homo-oligomer formation, in complex formation. Taken together, these findings provide new insights into the nature of nanometer-sized protein complexes in the autophagy pathway.

ARTICLE HISTORY

Received 7 April 2014
Revised 24 May 2016
Accepted 1 June 2016

KEYWORDS

autophagy; ATG8; diffusion; fluorescence; FRAP; FRET; hydrodynamic radius; MAP1LC3; SQSTM1



Introduction

Autophagy is a major degradation pathway whereby cytoplasmic contents are sequestered for degradation via the lysosome.¹ A conserved pathway in eukaryotes, autophagy is vitally important for normal health, development, and the prevention of disease.² In autophagy, the formation of a double-membrane intermediate compartment known as a phagophore is responsible for engulfing regions of cytoplasm; the phagophore subsequently matures into an autophagosome. Autophagy can occur either with or without substrate specificity, termed selective or nonselective autophagy, respectively. In selective autophagy, a ligand—such as ubiquitin—is conjugated to specific substrates, e.g. protein aggregates or mitochondria. Next, receptors and adaptors bind to the ubiquitinated substrate and target it to phagophore-associated Atg8 proteins.³ The autophagosome-encapsulated cargo is subsequently trafficked to the lysosome where its outer membrane subsequently fuses with the lysosome, thereby degrading its inner membrane and contents.^{1,4–6}


Among the members of the Atg8 protein family, the most widely studied protein is microtubule associated protein 1 light chain 3 β /LC3B. The known functions of LC3 include contributions to phagophore membrane expansion and fusion, and selective recruitment of cargo to the phagophore.⁷ LC3 is post-translationally modified on its C-terminal glycine residue with

the lipid phosphatidylethanolamine, and thus exists in 2 forms: a soluble form known as LC3-I, as well as a phagophore- and autophagosome-associated form known as LC3-II.^{8,9} The process of LC3 lipid modification is carried out through a series of enzymatic reactions resembling ubiquitination, but is reversible via the action of the cysteine proteinase ATG4B.¹⁰ Since LC3 itself is structurally similar to ubiquitin, it has been dubbed a ubiquitin-like protein.⁷ Interestingly, LC3 associates with slowly diffusing, high molecular weight complexes in both the cytoplasm and nucleus.^{11–14} Although the exact composition of these complexes is not yet known, their formation does not require lipidation of LC3.^{12,13} Nuclear LC3 is deacetylated in response to starvation and is subsequently trafficked to the cytoplasm where it initiates autophagosome formation.¹⁵ Under steady-state conditions, nuclear targeting of LC3 and its nucleocytoplasmic exchange is regulated by residues that make up its triple arginine motif and hydrophobic binding interface.¹³ Furthermore, nuclear LC3 associates with the nucleolus in a manner that depends on its triple arginine motif, and appears to interact with a variety of different nucleolar constituents including several 40S ribosomal proteins.¹³

Consistent with their central role in the autophagy pathway, LC3 and other Atg8 family members interact with a large network of more than 65 different proteins with extensive overlap

CONTACT Anne K. Kenworthy  Anne.kenworthy@vanderbilt.edu  Department of Molecular Physiology and Biophysics, 718 Light Hall, Vanderbilt University School of Medicine, Nashville, TN 37221, USA.

*Current affiliation: Department of Chemistry and Chemical Biology, Harvard University, Cambridge, MA, USA.

 Supplemental data for this article can be accessed on the publisher's website.

among Atg8 family members.¹⁶ Many of these interactions are mediated by a consensus LC3-interacting region (LIR) in the interacting proteins.¹⁷ SQSTM1/p62 (sequestosome 1) contains a LIR, and is one of the best-characterized LC3-interacting proteins.^{18,19} SQSTM1 homo-oligomerizes via its PB1 domain, and functions as a cargo receptor in selective autophagy.^{4,20} The interactions of SQSTM1 and LC3 have been studied extensively using a combination of co-immunoprecipitation, affinity isolation assays, structural analysis, mass spectrometry, and colocalization approaches.^{16,18,21–25} The results of these studies have revealed that SQSTM1—via its LIR domain—reversibly binds to LC3 in the region of residues F52 and L53.^{16,21,22,25,26} This binding does not, however, require lipidation of LC3, as a G120A mutant that disrupts LC3's lipidation coimmunoprecipitates with SQSTM1.²⁵ The interaction of SQSTM1 and LC3 is important for degrading ubiquitinated protein aggregates as well as degradation of SQSTM1 itself by autophagy.^{18,21,22,27,28} SQSTM1 binding to the N-terminal domain of LC3 has also been shown to inhibit 20S proteasome-mediated LC3 degradation.²⁹ SQSTM1 binding to LC3 alone, however, is not required to target SQSTM1 to sites of autophagosome formation.³⁰

SQSTM1 forms homo-oligomers and these homo-oligomers are crucial for several of its known activities. Mediated by its PB1 domain,^{31,32} homo-oligomerization of SQSTM1 is thought to be important for the formation of SQSTM1 inclusion bodies,¹⁸ interaction with LC3,¹⁸ targeting to phagophores,³⁰ and efficient recognition of ubiquitin and ubiquitinated cargo.^{33,34} Although the presence of SQSTM1 homo-oligomers in cells is often inferred from the formation of SQSTM1-positive inclusion bodies, diffuse cytoplasmic pools of SQSTM1 have also been proposed to consist of polymeric forms of the protein.³⁵ Until recently, very little was known about the structural organization of SQSTM1 homo-oligomers; however, in the past year, cryo-electron microscopy studies have revealed that SQSTM1 forms rod-like, helical filaments of nanometer size in vitro.³⁶ The properties of diffuse cytoplasmic SQSTM1 oligomers in cells, however, are not well understood. Furthermore, even though the interactions of LC3 and SQSTM1 in puncta have been extensively studied, much less is known about the nature of their interaction prior to puncta formation in live cells at the molecular level.

To address these questions, in the current study we investigated the properties of soluble SQSTM1 complexes and soluble complexes formed between SQSTM1 oligomers and LC3 using a combination of fluorescence microscopy-based biophysical approaches in living cells.

Results

Overexpression of SQSTM1 pulls LC3 out of the nucleus

As a model system for studying the size, organization, and dynamics of soluble (puncta-independent) complexes containing SQSTM1 and LC3, we constructed Cerulean- and Venus-labeled versions of both proteins and expressed them in HeLa cells in the presence of endogenous SQSTM1 and LC3. To measure the levels of overexpression of the fusion constructs relative to endogenous proteins, we quantified the relative amount of exogenous and endogenous proteins by western blotting

(corrected for the transfection efficiency). Under the conditions of our experiments, Venus-LC3 was expressed at ~60 times the level of endogenous LC3, while Venus-SQSTM1 was expressed at ~6-fold over endogenous levels (Fig. 1). As expected, co-expression of Cerulean-SQSTM1 with Venus-LC3 led to the recruitment of LC3 into SQSTM1-positive aggregates in the cytoplasm. Interestingly, this was accompanied by a dramatic redistribution of soluble Venus-LC3 from the nucleus to the cytoplasm (Fig. 2) ($p \leq 0.003$; Bonferonni corrected t test). We quantified the change in soluble LC3's nucleocytoplasmic (N/C) distribution across multiple cells using an automated image analysis routine, and found that it was reduced from 2.1 ± 0.2 to 1.37 ± 0.08 (Fig. 2C).

To verify the specificity of binding of LC3 to SQSTM1, we utilized several mutant forms of LC3. These included an LC3^{G120A} mutant, which is incapable of lipid modification, and association with puncta;^{8,37} LC3^{R70A}, a mutant that exhibits decreased binding to a subset of LC3-interacting proteins;¹⁶ and LC3^{F52A,L53A}, another mutant that undergoes decreased binding to a subset of LC3-interacting proteins including SQSTM1.¹⁶ F52 and L53 are also close to residues K49 and K51—sites of acetylation that regulate LC3's N/C transport via binding to DOR.¹⁵ Previous studies have indicated that SQSTM1 is capable of binding to G120A and R70A, but shows greatly reduced binding to F52A and L53A mutants.^{16,22,25,33}

As for the case of wild-type Venus-LC3, Venus-LC3^{G120A} and Venus-LC3^{R70A} were recruited to SQSTM1-positive puncta and were shifted out of the nucleus in cotransfected cells (Fig. 2B and C). Venus-LC3^{F52A,L53A}, however, neither associated with puncta nor showed any change in its N/C ratio (Fig. 2B and C). Thus, in addition to binding to SQSTM1-induced puncta, changes in the N/C distribution of soluble LC3 occur as the result of its interactions with overexpressed SQSTM1.

SQSTM1 and LC3 are in close physical proximity in the cytoplasm and in aggregates as measured by FRET

To more directly study the interaction of the soluble pools of SQSTM1 and LC3, we turned to FRET. Direct protein-protein interactions bring proteins within close physical proximity of one another and thus can be monitored using FRET.^{38–41} To measure FRET between Cerulean- and Venus-tagged versions of LC3 and SQSTM1, we used acceptor photobleaching, a well-characterized method to quantify energy transfer by fluorescence microscopy.^{14,42–47}

In our experiments, we measured FRET between Cerulean-SQSTM1 and the various Venus-LC3 constructs separately for the diffuse cytoplasmic pool of the proteins and in puncta (Fig. 3). Soluble Cerulean-SQSTM1 and wild-type Venus-LC3, Venus-LC3^{G120A}, or Venus-LC3^{R70A} undergo significant FRET, which is indicative of their close proximity ($p \leq 0.01$; t -test) (Fig. 3A). Similar energy transfer efficiency (E) values were measured in puncta between Cerulean-SQSTM1 and either wild-type Venus-LC3 or Venus-LC3^{G120A} (Fig. 3B). On the other hand, E measured between Cerulean-SQSTM1 and the Venus-LC3^{F52A,L53A} mutant was no different than background, suggesting, in fact, the F52A L53A mutation disrupts association with SQSTM1 ($p > 0.01$; t -test). Our FRET results demonstrate that Cerulean-SQSTM1

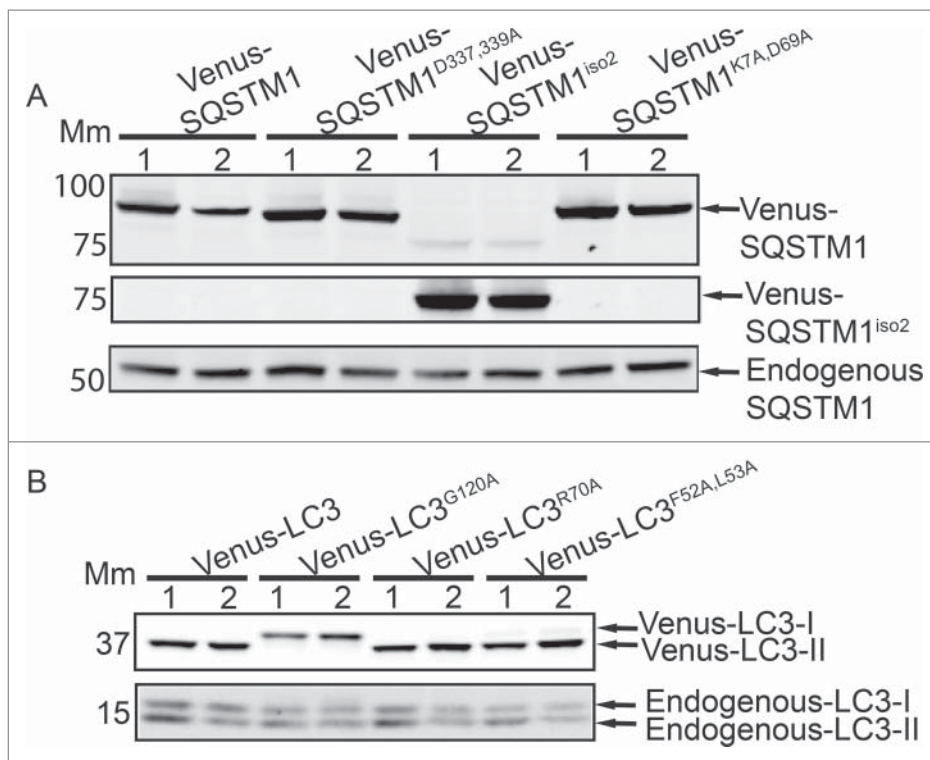


Figure 1. Western blot showing the relative expression levels of the Venus tagged SQSTM1 and LC3 constructs compared to endogenous SQSTM1 and LC3. HeLa cells transfected with the indicated Venus-tagged SQSTM1 or LC3 constructs in duplicate were lysed and resolved by SDS-PAGE followed by western blotting with (A) anti-SQSTM1 or (B) anti-LC3 antibodies. Mm, molecular mass markers in kilodaltons.

and Venus-LC3 are not only associating with one another in puncta, but that the soluble forms of the 2 proteins also appear to interact in the cytoplasm.

LC3 forms a large complex with overexpressed SQSTM1, as measured by diffusion

We next asked whether binding of SQSTM1 to LC3 leads to a change in the size of LC3-associated protein complexes. Because SQSTM1 contains an LC3 binding site, forms homooligomers, and binds to ubiquitinated autophagy substrates,^{4,48} we hypothesized that it should form a complex with LC3, which has a much larger hydrodynamic radius than that of unbound LC3. Furthermore, a large complex between LC3 and SQSTM1 should not be observed for the Venus-LC3^{F52A,L53A} mutant, which is incapable of binding to SQSTM1.

To address this question, we took advantage of a quantitative confocal FRAP assay directed at the soluble pool of the proteins to quantify their diffusion coefficient—a constant that is inversely related to molecular size. In this assay, we use a small circular 1- μm radius bleach region placed in a relatively homogeneous region of the cytoplasm so as to avoid any bright puncta.¹² These experiments thus measure the diffusional mobility of soluble pools of LC3 and SQSTM1, as opposed to turnover of the 2 proteins on puncta.⁴⁴ Using the Stokes-Einstein equation, it is possible to estimate the apparent molecular weight of the soluble complexes associated with each protein assuming a spherical geometry ($D \sim MW^{-1/3}$, with Venus as a standard for MW).^{12,14}

As a starting point, we measured D for cytoplasmic Venus, which should diffuse as a monomer with an expected molecular mass of ~ 27 kDa, and should not form a complex with SQSTM1. We obtained a D of $35 \pm 3 \mu\text{m}^2/\text{s}$ for Venus, whereas the mobile fraction was near 100% for Venus, as expected based on its ability to freely diffuse. In addition, we did not observe a change in its D in the presence of SQSTM1 ($p > 0.01$; t test) (Fig. 4B).

We next measured the diffusional mobility of Venus-LC3 and the Venus-LC3 mutants in the presence and absence of overexpressed SQSTM1. Examples of experimental FRAP curves and fits with a diffusion model are shown for Venus-LC3 in the presence and absence of overexpressed SQSTM1 (Fig. 4A). When co-expressed with Cerulean, the diffusional mobility of the different Venus-LC3 mutants differed significantly from one another (Fig. 4 and Table 1), as was described in our recent report documenting the sizes of Venus-LC3-associated protein complexes in the cytoplasm of living cells and cytoplasmic extracts.¹² In the presence of overexpressed SQSTM1, our FRAP measurements showed a significant reduction in D for wild-type Venus-LC3, Venus-LC3^{G120A}, and Venus-LC3^{R70A} compared to cells co-expressing Cerulean ($p \leq 0.01$; t -tests), whereas the D for the Venus-LC3^{F52A,L53A} mutant was unchanged in the presence of overexpressed SQSTM1 (Fig. 4B) ($p > 0.01$; t test). We estimated the size of each of the Venus-LC3-Cerulean-SQSTM1-associated complexes using the Stokes-Einstein relation, as summarized in Table 1. These results are in good agreement with our N/C measurements and FRET measurements, which altogether suggest that overexpressed SQSTM1—via its LC3 binding site—forms a large, soluble (puncta-independent) complex with Venus-LC3 in the cytoplasm.

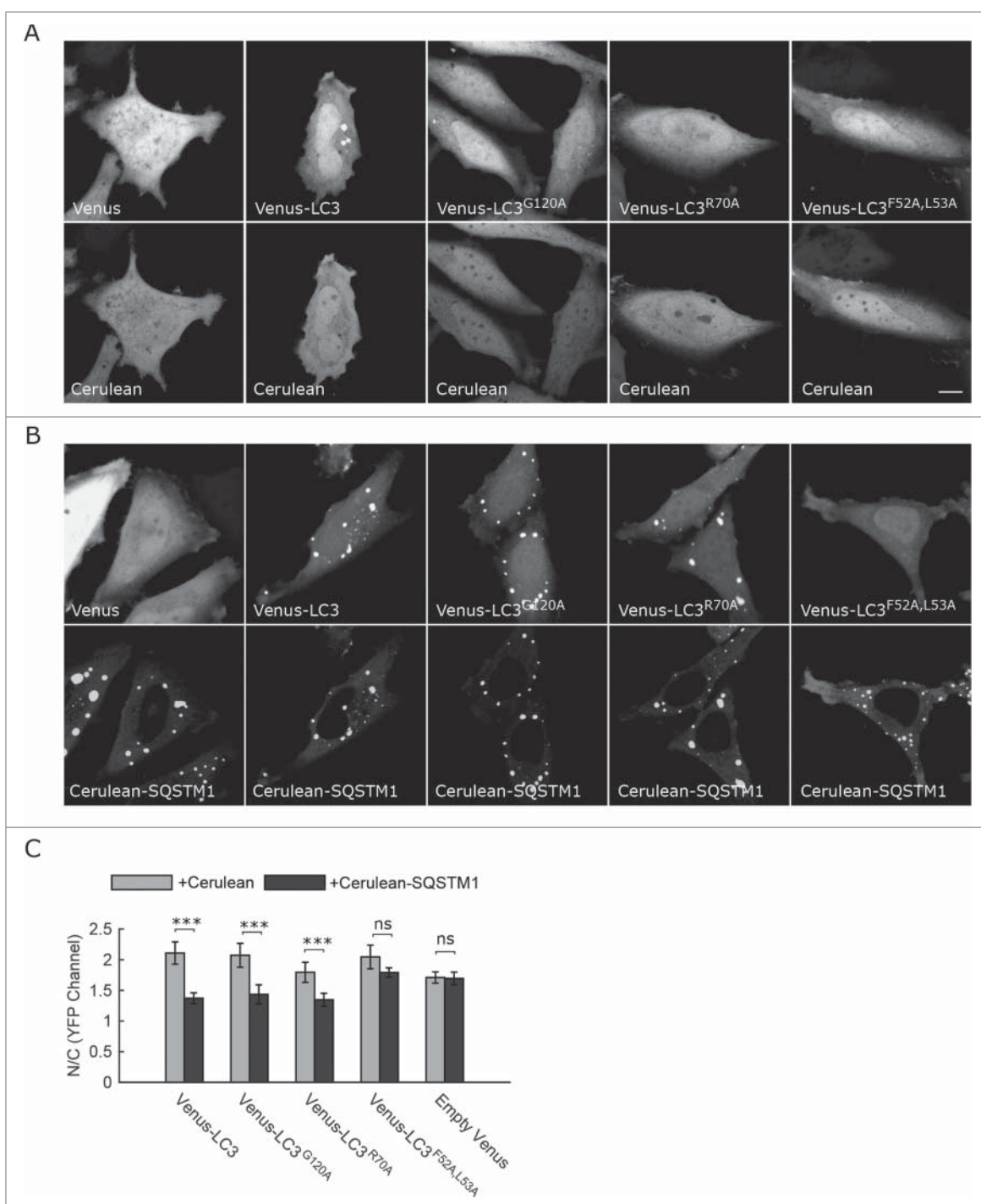


Figure 2. The nucleocytoplasmic ratio of soluble Venus-LC3 is decreased in the presence of overexpressed Cerulean-SQSTM1. Representative confocal images of the localization of Venus, Venus-LC3, Venus-LC3^{G120A}, Venus-LC3^{F52A,L53A}, and Venus-LC3^{R70A} when transiently co-expressed with (A) Cerulean or (B) Cerulean-SQSTM1 in HeLa cells. Scale bar: 10 μ m. (C) An automated image analysis routine was used to quantify the N/C ratio of the soluble (puncta independent) Venus fluorescence (YFP channel) in the cells co-expressing the indicated Venus-tagged constructs in combination with either Cerulean (light gray bars) or Cerulean-SQSTM1 (dark gray bars). Bars are the mean \pm 95% confidence interval for N = 20 cells from 2 independent experiments. Statistical comparisons are between the grouped bars. ns, $p > 0.05$; ***, $p \leq 0.001$.

The soluble LC3-SQSTM1 complexes form via a mechanism that depends on SQSTM1's LIR domain, but not its PB1 domain

In order to investigate the properties of the large, soluble SQSTM1-LC3 complexes further, we carried out additional experiments—using the set of methods presented above—on a series of SQSTM1 mutants. The SQSTM1 constructs that we

examined included: (i) a LIR mutant (D337-339A) that was reported to disrupt its ability to bind to LC3;^{22,30} (ii) a PB1 domain mutant of LC3 (K7A D69A) that disrupts SQSTM1 polymerization;^{31,35} and (iii) human SQSTM1 isoform 2 (iso2), which is generated by alternative splicing and is missing a major portion of the PB1 domain required for self-association.⁴⁹ In addition, inhibition of SQSTM1's ability to homo-oligomerize via mutation of its PB1 domain has been reported to

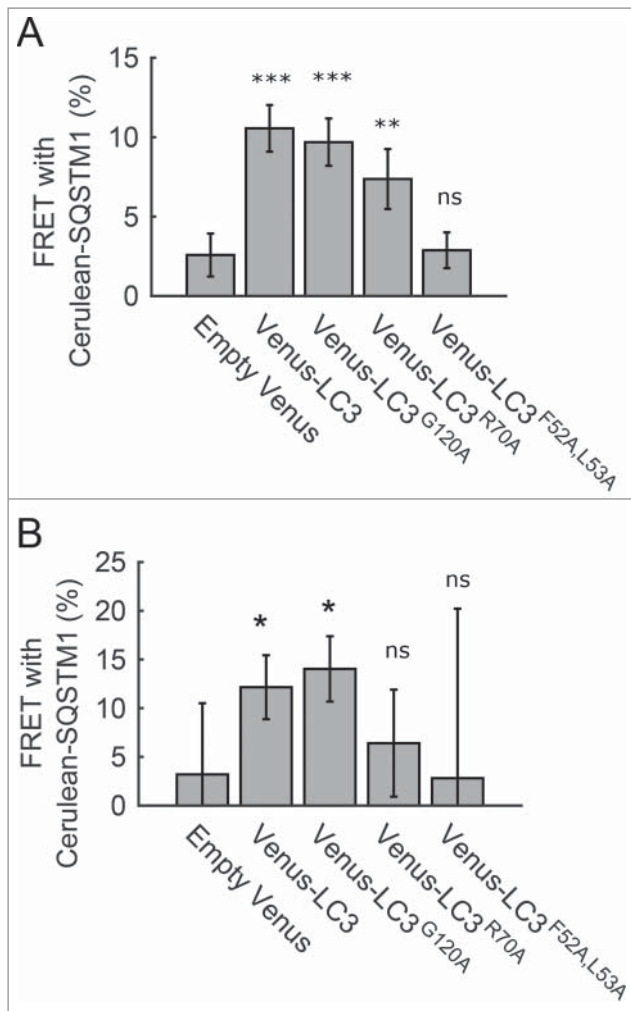


Figure 3. FRET reports on the close physical proximity of both soluble and puncta-associated Cerulean-SQSTM1 and Venus-LC3. FRET analysis was performed on cells co-expressing Cerulean-SQSTM1 with the indicated Venus-LC3 constructs and semi-automatically analyzed across multiple cells. The data were separately analyzed for (A) soluble SQSTM1 and (B) puncta-associated pools of SQSTM1. FRET was also measured between Cerulean-SQSTM1 and empty Venus as a negative control. Bars are the mean \pm 95% confidence interval for $N = 9$ –30 cells from 3 independent experiments. Statistical comparisons are with the negative control. ns, $p > 0.05$; *, $p \leq 0.05$; **, $p \leq 0.01$; ***, $p \leq 0.001$.

significantly decrease its interaction with LC3 as assessed by immunoprecipitation,¹⁸ although more recent results suggest that LC3 can in fact interact with non-oligomerized forms of SQSTM1.³⁴

We verified the expression levels of the various SQSTM1 constructs by western blotting and found that all were expressed at ~6- to 7-fold higher levels than endogenous SQSTM1 (Fig. 1). Thus, under the conditions of our experiments, the SQSTM1 constructs were expressed in excess over endogenous SQSTM1, but endogenous SQSTM1 was still present. We first asked if LC3 is pulled out of the nucleus by overexpressed PB1 domain mutants of SQSTM1. When transiently expressed in HeLa cells either in the absence or presence of overexpressed LC3, the PB1 domain mutants, Venus-SQSTM1^{K7A,D69A} and Venus-SQSTM1^{iso2}, did not form puncta, and were present in a soluble form in the cytoplasm, whereas the LIR mutant, Venus-SQSTM1^{D337-339A}, retained the ability to form large aggregates (Fig. 5A). Strikingly, in the presence of overexpressed Cerulean-SQSTM1^{K7A,D69A} or

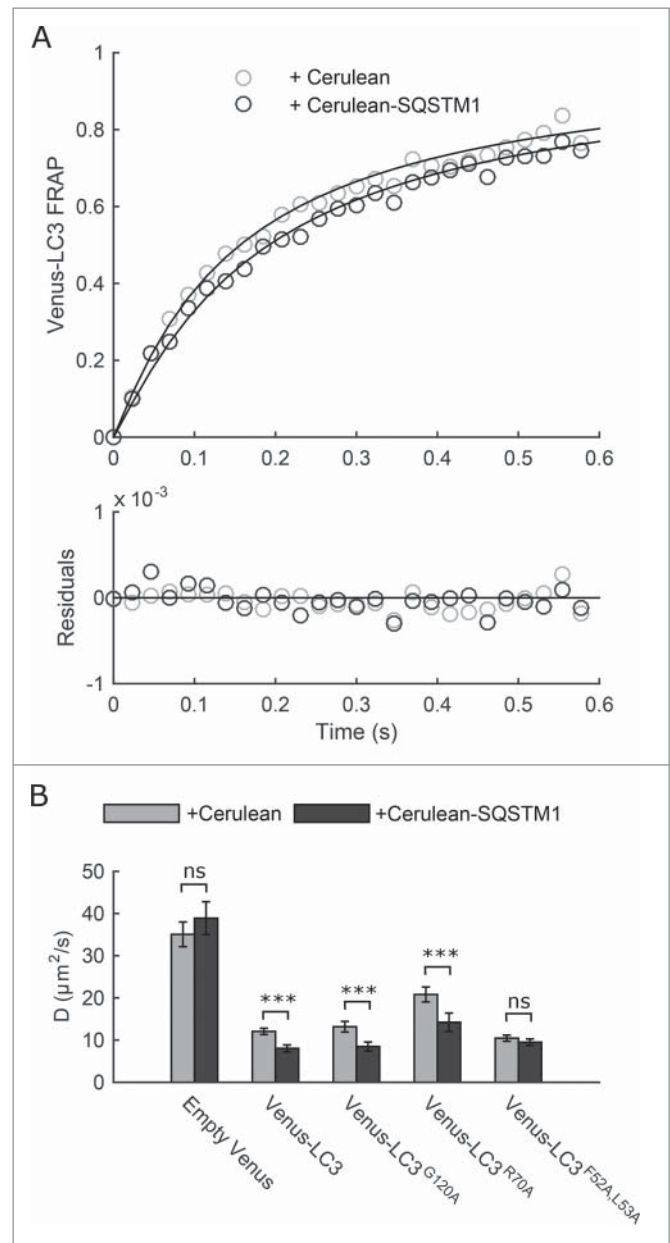


Figure 4. Venus-LC3's rate of diffusion decreases when co-expressed with Cerulean-SQSTM1. A quantitative FRAP assay was carried out on cells co-expressing the indicated Venus- and Cerulean-tagged constructs using a rectangular imaging ROI centered on the cytoplasm, and small circular bleach region ($r_b = 1 \mu\text{m}$) placed in a region devoid of puncta. (A) Examples of the early time-points from normalized FRAP recoveries are shown for Venus-LC3 co-expressed with Cerulean (light gray circles) or with Cerulean-SQSTM1 (dark gray circles). The solid lines are fits to a single component diffusion model. Residuals for the fits are indicated in the lower panel. (B) D values for the indicated Venus-LC3 constructs in cells co-expressing either Cerulean (light gray bars) or Cerulean-SQSTM1 (dark gray bars). Empty Venus was included as a control. Bars show the mean \pm 95% confidence intervals for $N = 19$ –64 cells from 2–4 independent experiments. Statistical comparisons are between the grouped bars. ns, $p > 0.05$; ***, $p \leq 0.001$.

Cerulean-SQSTM1^{iso2}, Venus-LC3 was pulled out of the nucleus into the cytoplasm to the same extent as in cells expressing wild-type Cerulean-SQSTM1, even though these mutant forms of Cerulean-SQSTM1 were unable to form puncta (Fig. 5A and B). Conversely, the LIR mutant, Cerulean-SQSTM1^{D337-339A} was less capable of changing Venus-LC3's N/C distribution. The LIR mutant, however, may still weakly interact either directly or indirectly with LC3, as it retained the ability to pull Venus-LC3 out of

Table 1. Apparent molecular mass and mobile fractions for Venus, Venus-LC3, and Venus-LC3 mutants co-expressing either Cerulean or Cerulean-SQSTM1 based on the FRAP diffusion measurements in live HeLa cells under basal conditions.

Construct	ζ Apparent Mm (kDa)	Mobile Fraction (%)
Venus		
+ Cerulean	N/A	100 ± 1 (35)
Venus-LC3		
+ Cerulean	600 ± 200 (64)	99.9 ± 0.9 (64)
+ Cerulean-SQSTM1	2200 ± 800 (30)	100 ± 2 (30)
Venus-LC3 ^{G120A}		
+ Cerulean	500 ± 200 (30)	100 ± 1 (30)
+ Cerulean-SQSTM1	1900 ± 800 (30)	99 ± 1 (30)
Venus-LC3 ^{F52A,L53A}		
+ Cerulean	1000 ± 300 (32)	100 ± 1 (32)
+ Cerulean-SQSTM1	1400 ± 500 (30)	99 ± 1 (30)
Venus-LC3 ^{R70A}		
+ Cerulean	130 ± 40 (29)	100 ± 1 (29)
+ Cerulean-SQSTM1	400 ± 200 (30)	99 ± 2 (30)
Venus-SQSTM1		
+ Cerulean-SQSTM1	9 × 10 ⁴ ± 9 × 10 ⁴ (20)	97 ± 2 (20)

ζ assuming a spherical geometry. ±95% confidence intervals (N = # cells).

the nucleus compared to cells co-expressing Cerulean. Weak interactions between the 2 may also explain the small amount of Venus-LC3 colocalized with Cerulean-SQSTM1^{D337-339A} puncta (Fig. 5A).

SQSTM1 bears both an active nuclear export signal and an active nuclear import signal, which it uses to shuttle between the cytoplasm and nucleus.³⁵ In addition, SQSTM1's N/C transport reportedly depends on the oligomerization state of the protein.³⁵ We took advantage of this active N/C shuttling of SQSTM1 to additionally test for the formation of complexes between soluble LC3 and SQSTM1. We first confirmed that Venus-SQSTM1 redistributes into the nucleus after treatment with an XPO1/exportin1-mediated active nuclear export inhibitor, leptomycin B (LMB) (Fig. 6A and B). The PB1 domain mutants, SQSTM1^{K7A,D69A} and SQSTM1^{iso2} were the most strongly redistributed, whereas wild-type SQSTM1 and SQSTM1^{D337-339A} were partially retained in the cytoplasm (Fig. 6B). This suggests that a high affinity for puncta competes with the active import of Venus-SQSTM1 into the nucleus upon treatment with LMB.

To test whether shuttling of SQSTM1 into and out of the nucleus can lead to a corresponding redistribution of LC3, we focused on the N/C ratio of LC3 in cells co-expressing human SQSTM1^{iso2} (a construct that does not form puncta) after treatment with LMB (Fig. 7A and B). We co-expressed SQSTM1^{iso2} together with each of the LC3 mutants that we examined above with SQSTM1. In addition, we examined a NES-Venus-LC3 construct bearing an N-terminal nuclear export signal, as this

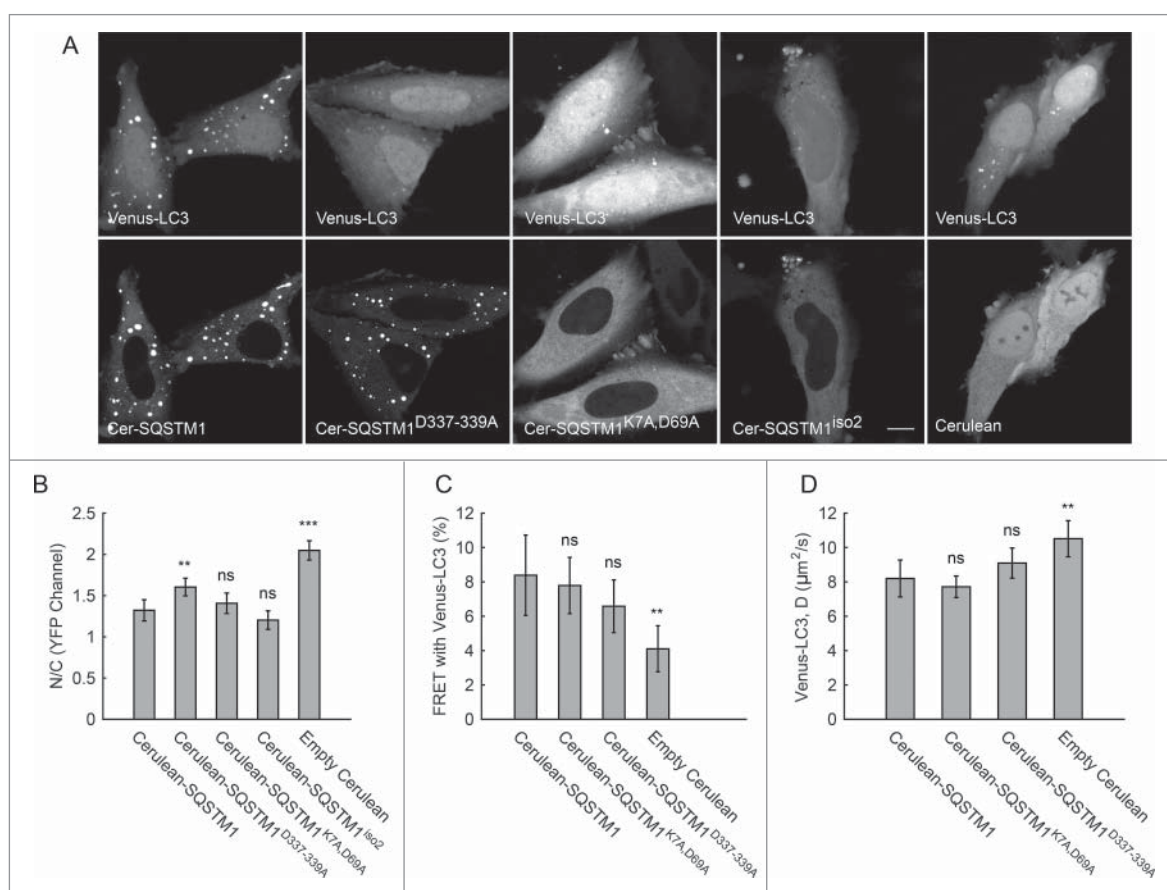


Figure 5. Soluble Venus-LC3 interacts with overexpressed Cerulean-SQSTM1 even when SQSTM1's PB1 domain is disrupted. (A) Representative confocal images of the localization of Venus-LC3 in HeLa cells co-expressing either Cerulean, as a negative control, or the indicated Cerulean-SQSTM1 constructs. Scale bar: 10 μm. (B) Quantification of the N/C ratios for soluble Venus-LC3 (YFP channel) in the presence of the indicated constructs. Bars show the mean ± 95% confidence intervals for N = 20–31 cells from 2–3 independent experiments. (C) Quantification of FRET between soluble Venus-LC3 and the indicated Cerulean-SQSTM1 constructs. FRET between Venus-LC3 and Cerulean was assessed as a negative control. Bars show the mean ± 95% confidence intervals for N = 30 cells from 3 independent experiments. (D) D for Venus-LC3 in cells co-expressing the indicated Cerulean-SQSTM1 constructs or empty Cerulean. Bars show the mean ± 95% confidence interval for N=30–35 cells from 3 independent experiments. Statistics are for comparisons with Venus-LC3 co-expressing wild-type SQSTM1. ns, p > 0.05; **, p ≤ 0.01; ***, p ≤ 0.001.

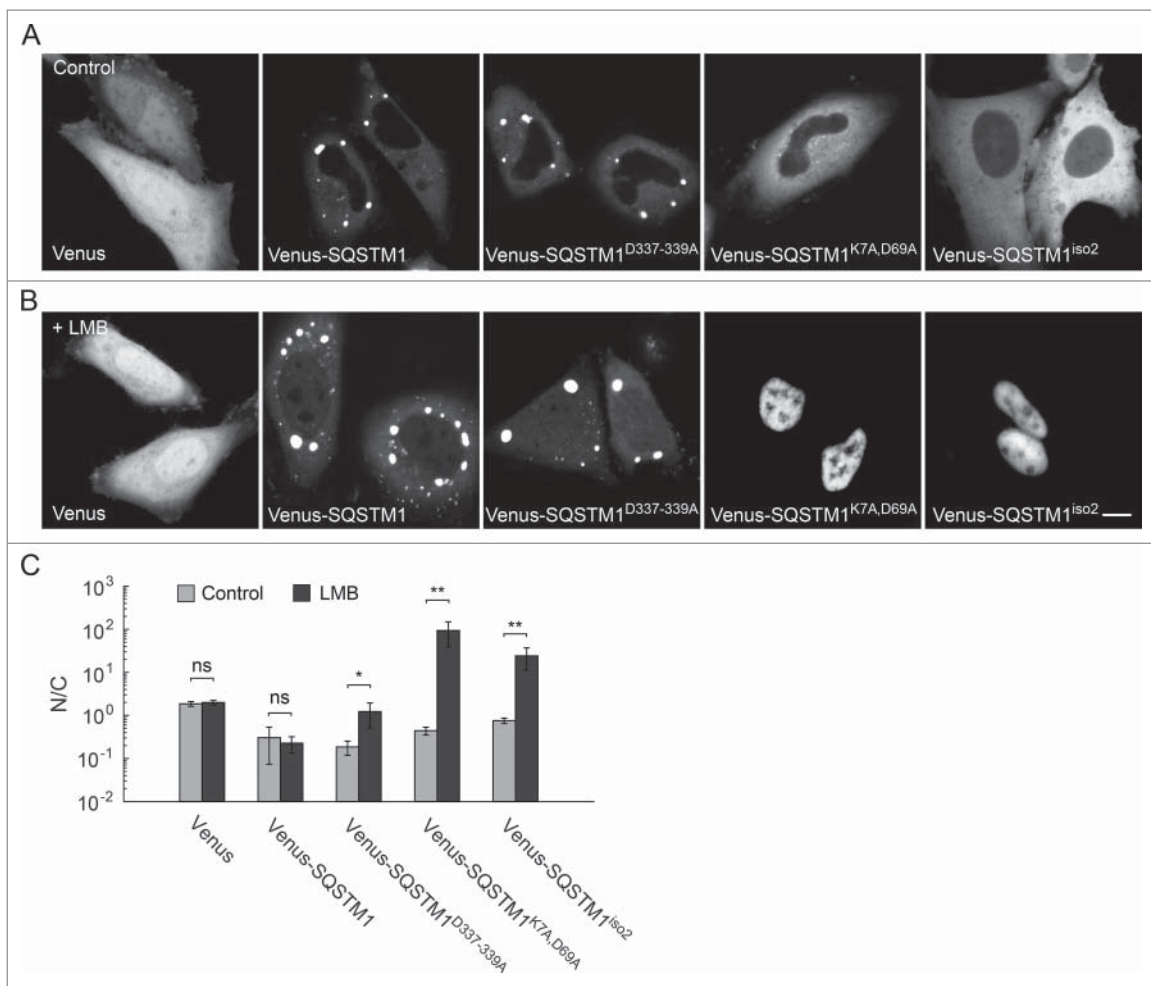


Figure 6. Nucleocytoplasmic distribution of Venus-SQSTM1 constructs. Representative images of the subcellular distribution of the indicated SQSTM1 and SQSTM1 isoform 2 constructs (A) following 2 h in the presence of vehicle or (B) following 2 h of LMB treatment. Scale bar: 10 μ m. Data are representative of 3 independent experiments. (C) A semi-automated image analysis routine was used to quantify the N/C ratio of the soluble (puncta independent) Venus fluorescence (YFP channel) in the cells expressing the indicated Venus-tagged SQSTM1 constructs and nuclei labeled with DRAQ5 in the absence of LMB (light gray bars) or presence of LMB (dark gray bars). Bars are the mean \pm 95% confidence interval for N = 20 cells from 2 independent experiments. ns, $p > 0.05$; *, $p \leq 0.05$; **, $p \leq 0.01$.

protein is present in the nucleus only in small amounts under basal conditions. Again, we found that each Venus-LC3 construct was robustly pulled out of the nucleus under control conditions, with the exception of Venus-LC3^{F52A,L53A} (Fig. 7A). Finally, we found that in cells co-expressing SQSTM1^{iso2} with NES-LC3, LC3, LC3^{G120A}, or LC3^{R70A}, treatment with LMB resulted in substantial redistribution of LC3 into the nucleus ($p \leq 0.01$; *t* tests). Conversely, Venus-LC3^{F52A,L53A} only modestly redistributed in LMB-treated cells expressing SQSTM1^{iso2}, again demonstrating its less efficient binding to SQSTM1^{iso2}.

We further analyzed the interactions of the soluble cytoplasmic pools of Venus-LC3 and the Cerulean-SQSTM1 constructs using FRET (Fig. 5C) and FRAP (Fig. 5D). We observed similar levels of FRET between soluble Venus-LC3 and Cerulean-SQSTM1, Venus-LC3 and Cerulean-SQSTM1^{K7A,D69A}, and Venus-LC3 and Cerulean-SQSTM1^{D337-339A}. All levels of FRET were significantly higher than that measured between Venus-LC3 and Cerulean ($p > 0.01$; *t*-tests) (Fig. 5C). Thus, both the SQSTM1 PB1 domain mutant and LIR mutant appear to be in close physical proximity to LC3. FRAP studies reported similar effects on the formation of large complexes between overexpressed SQSTM1 mutants and LC3 (Fig. 5D). Compared to *D* for Venus-LC3 in cells co-

expressing Cerulean, *D* for Venus-LC3 was significantly decreased in cells co-expressing Cerulean-SQSTM1, Cerulean-SQSTM1^{K7A,D69A}, and Cerulean-SQSTM1^{D337-339A} ($p > 0.01$; *t*-tests) (Fig. 5D).

Taken together, these results show that soluble LC3 and SQSTM1 form large, soluble complexes in the cytoplasm that are independent of puncta.

Analysis of soluble SQSTM1 homo-oligomers in cells

A recent *in vitro* structural analysis showed that SQSTM1 homo-oligomerizes via its PB1 domain to form long, rod-like complexes with a width of 15 nm and a length of about 40 nm.³⁶ This is intriguing in the context of our analysis of SQSTM1-LC3 complexes, because these large SQSTM1 rods have many LC3 binding sites, and thus may correspond to the complexes that we observed in cells overexpressing SQSTM1.

In order to test this hypothesis, we first asked if measurable FRET occurs between soluble Cerulean-SQSTM1 and Venus-SQSTM1 (Fig. 8A and B). We quantified *E* for both the soluble pools of SQSTM1 and the puncta-associated protein. Consistent with previous reports,⁴⁴ we found that Venus-SQSTM1 and Cerulean-SQSTM1 associated with puncta exhibit substantial FRET

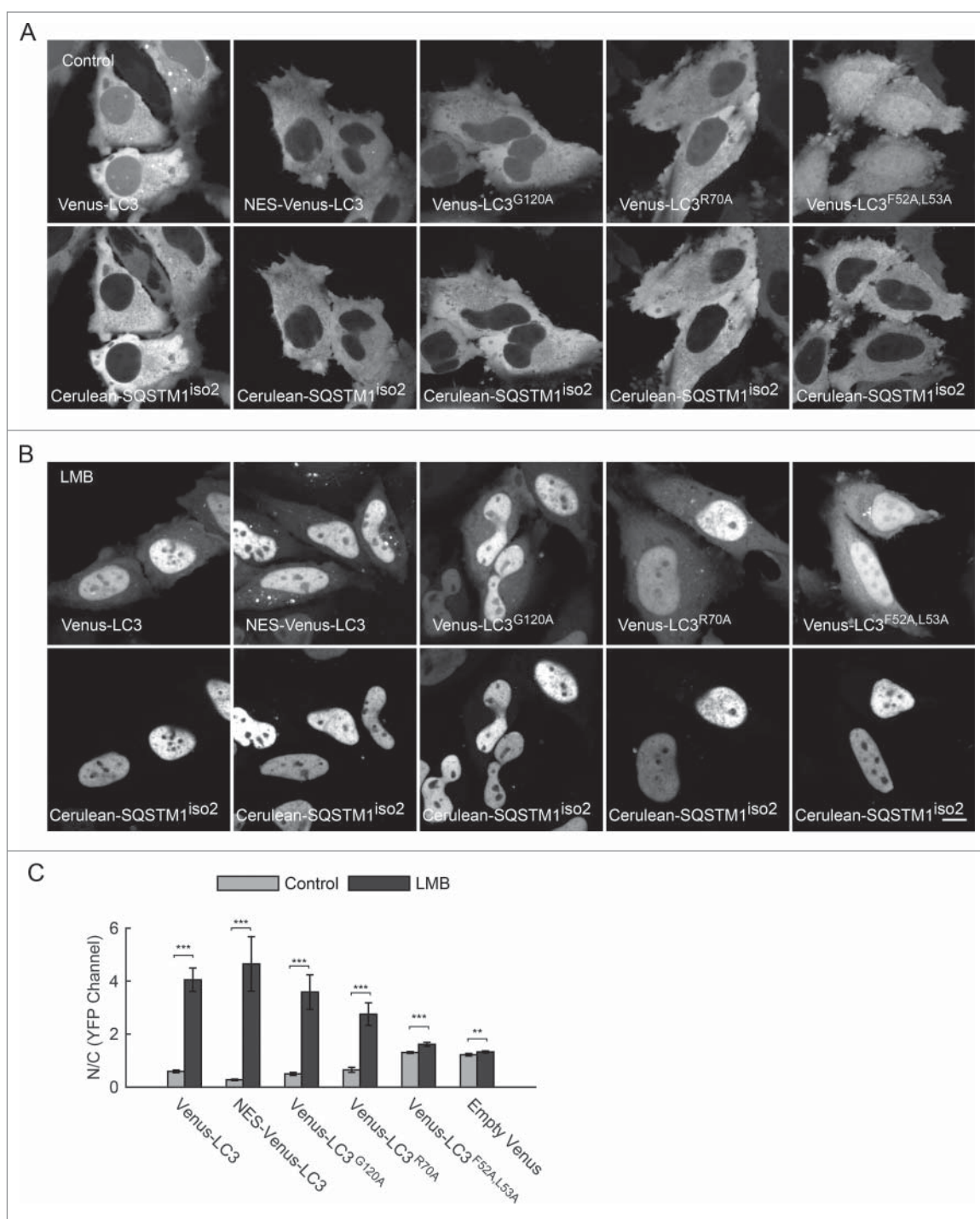


Figure 7. When co-expressed with Cerulean-SQSTM1^{iso2}, Venus-LC3 redistributes from the cytoplasm to the nucleus in response to LMB treatment. Representative images of the indicated Venus-LC3 constructs in the presence of overexpressed Cerulean-SQSTM1^{iso2}. (A) after 2 h in the presence of vehicle or (B) after 2 h of LMB treatment. Scale bar: 10 μ m. (C) Quantification of the N/C ratios for the indicated Venus-LC3 constructs (YFP channel) in cells co-expressing Cerulean-SQSTM1^{iso2} in the absence of LMB (light gray bars) or presence of LMB (dark gray bars). Bars show the mean \pm 95% confidence intervals for N = 18–64 cells from 1–3 independent experiments. **, $p \leq 0.01$; ***, $p \leq 0.001$.

compared to a negative control—cells expressing Cerulean-SQSTM1 and Venus ($p \leq 0.01$; *t* test) (Fig. 8A). In addition, we observed substantial homo-FRET for soluble SQSTM1 ($p \leq 0.01$; *t* test) (Fig. 8A). FRET for the SQSTM1^{D337-339A} LIR mutant, which contains an intact PB1 domain, was similar to that of the wild-type protein ($p > 0.01$; *t*-test) (Fig. 8A). Surprisingly, substantial FRET was also detected between the PB1 domain mutants Venus-SQSTM1^{K7A,D69A} and Cerulean-SQSTM1^{K7A,D69A} (Fig. 8), as well as for Venus-SQSTM1^{iso2} and Cerulean-SQSTM1^{iso2} (Fig. 8B).

Thus, even upon disruption of the PB1 domain of SQSTM1, multiple copies of tagged SQSTM1 remain within FRET proximity of one another in soluble complexes.

We next used FRAP to assess the apparent size of the SQSTM1 oligomers (Fig. 8C and D). Our FRAP measurements on the soluble (puncta-independent) pool of Venus-SQSTM1 revealed that, indeed, the protein diffuses slowly with a D of $4 \pm 1 \mu\text{m}^2/\text{s}$, and a mobile fraction of 100%, which suggests the protein is diffusing as a very large soluble complex. Assuming a spherical geometry, this

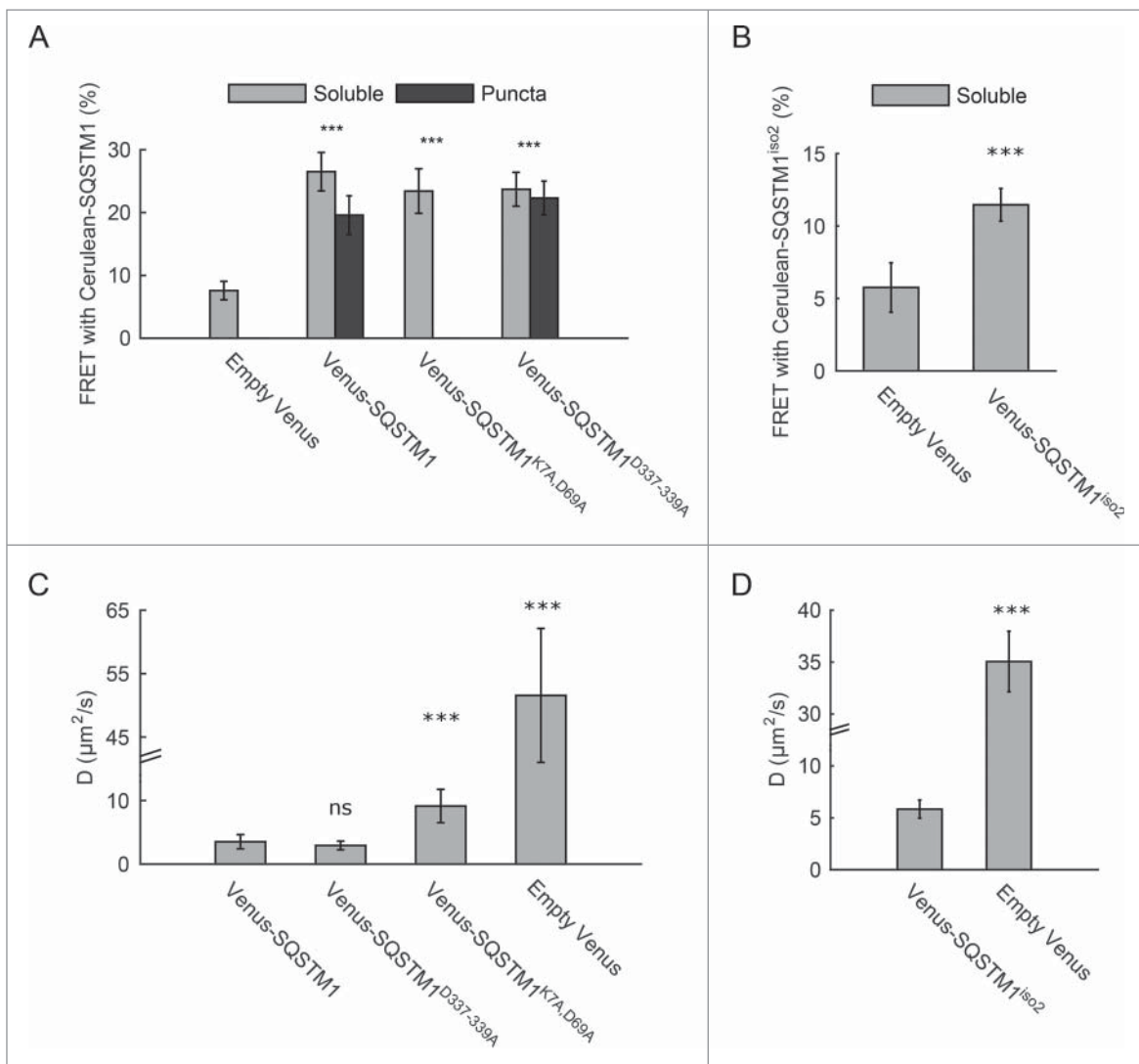


Figure 8. FRET and FRAP analysis of soluble SQSTM1 homo-oligomers. Analysis of FRET between Cerulean- and Venus-tagged versions of the indicated (A) SQSTM1 constructs, or (B) SQSTM1^{iso2}. FRET was separately calculated for the soluble pools of protein (light gray bars) and puncta-associated pools (dark gray bars). FRET was also measured in cells co-expressing Cerulean-SQSTM1 and empty Venus as negative controls. Bars show the mean \pm 95% confidence intervals for $N = 27$ – 30 cells from 3 independent experiments in (A), or $N = 20$ cells from 2 independent experiments in (B). Statistics are for the comparisons with the negative controls. FRAP analysis was used to quantify the diffusion coefficients of the indicated (C) Venus-tagged SQSTM1 constructs or (D) Venus-SQSTM1^{iso2}. Diffusion coefficients for empty Venus were measured as internal controls. Bars show the mean \pm 95% confidence intervals for $N = 10$ – 20 cells from 2 independent experiments in (A), and $N = 31$ – 35 cells from 3 independent experiments in (B). Statistics are for the comparisons with wild-type SQSTM1. ns, $p > 0.05$; ***, $p \leq 0.001$.

D value corresponds to a complex with an apparent size of nearly 90 MDa (Table 1). We were, however, interested to compare our measured D for SQSTM1 to the theoretical D for a rod-like complex with the dimensions that were reported in a recent *in vitro* structural analysis.³⁶ Using the published SQSTM1 rod dimensions (width = 15 nm, length = 40 nm), the known size and D of spherical Venus, and the published relationship between D and the size of a rod,⁵⁰ we calculated a theoretical D of $6 \mu\text{m}^2/\text{s}$ for the SQSTM1 rod-like complex—a value that is in remarkably good agreement with our live cell measurements.

The formation of oligomeric rods, however, depends on SQSTM1's PB1 domain, whereas binding to LC3 depends on the LIR domain; therefore, in order to test this further, we next examined the diffusion of the mutant SQSTM1 constructs. Surprisingly, we found that D for Venus-SQSTM1^{D337-339A} was statistically indistinguishable from wild-type SQSTM1 ($p > 0.01$; t test) and D for Venus-SQSTM1^{iso2} was similarly slow. D for

the Venus-SQSTM1^{K7A,D69A} mutant was statistically faster than wild-type Venus-SQSTM1, but again was very slow compared to the mobility of Venus ($p \leq 0.01$; t test) (Fig. 8C). On the basis of these findings, we conclude that soluble Venus-SQSTM1 associates with slowly diffusing complexes containing multiple copies of tagged SQSTM1. These soluble complexes are even observed under conditions when SQSTM1 is unable to form large insoluble aggregates in cells, for example as the result of mutation of the PB1 domain of SQSTM1 and when a major portion of the PB1 domain is missing in SQSTM1^{iso2}.

Discussion

It is well known that SQSTM1 functions as a homo-oligomeric selective autophagy receptor and that LC3 forms complexes with SQSTM1 that facilitate the delivery of cargo to phagophores, but the properties of these complexes in living cells remain poorly

understood. Here, we used a combination of localization, FRET, and FRAP to investigate SQSTM1 homo-oligomeric complexes and soluble (puncta-independent) complexes containing both LC3 and SQSTM1. Our studies primarily focused not on the previously well-described autophagosome associated pools of LC3 and SQSTM1, but rather on the soluble (diffusely distributed pool), independent of puncta. Thus, we probed the properties of dynamic protein complexes on a size scale that is not accessible by virtually any other method in live cells.

Our results reveal several new insights into the properties of soluble SQSTM1 homo-oligomers. Our FRET measurements show that multiple copies of SQSTM1 are in close proximity in living cells. These findings support previous proposals that even the soluble pools of SQSTM1 consist of polymers. We also found that soluble SQSTM1's diffusion coefficient is extremely slow for a soluble protein. This is consistent with SQSTM1's association with high molecular weight complexes as detected by size exclusion chromatography of purified recombinant SQSTM1 homo-oligomers,³² or as measured in cell lysates.³⁰ The size of the SQSTM1-containing complexes implied by our FRAP measurements is remarkably large; assuming the SQSTM1-associated complexes are spherical, they would be predicted to have an ~ 30 -nm radius. This slowly diffusing species could thus in principle correspond to very large complexes consisting of large homo-oligomers of SQSTM1 bound to selective autophagy substrates. Experiments utilizing UBA domain mutants of SQSTM1 could be used to test this further in future studies. A rod-shaped filament—such as the proposed structure of SQSTM1 oligomers from a recent cryo-electron microscopy study³⁶—would also be expected to have a diffusion coefficient that is similar to the one that we measured. SQSTM1 is also capable of interacting with multiple binding partners, which could also potentially be contained within these complexes. For example, in addition to its interactions with a variety of signaling proteins,⁵¹ SQSTM1 also associates with MTORC1 complexes.⁵² The slowly diffusing SQSTM1 complexes inferred from our findings could also potentially be associated with other large macromolecular structures such as proteasomes—structures measuring approximately 14 nm on their longest dimension⁵³—given that in addition to its role in selective autophagy, SQSTM1 is involved in shuttling ubiquitinated cargo to the proteasome for degradation and directly binds to the proteasome in this process.⁵⁴

Surprisingly, we detected FRET between PB1 domain mutants of SQSTM1, as well as for SQSTM1 isoform 2, which essentially lacks a functional PB1 domain. In addition, D was similarly low for wild-type SQSTM1 and the PB1 domain mutant, suggesting the mutant also associates with very large complexes of a similar size. This finding was despite the fact that the PB1 domain mutant and SQSTM1 isoform 2 did not form visible puncta—a characteristic that has been interpreted to reflect SQSTM1's ability to homo-oligomerize.^{18,30,35} This result was unexpected given previous reports that homo-oligomerization of SQSTM1 is dependent on the PB1 domain and that the ability of SQSTM1 to form helical filaments depends on the PB1 domain.³⁶ This finding is unlikely to be the result of direct interactions of the PB1 domain mutants of SQSTM1 with endogenous SQSTM1, since previous studies have reported that a K7A D69A mutant and wild-type SQSTM1 fail to interact.³¹ One potential explanation for these findings is

that multiple copies of the PB1 domain mutants of SQSTM1 may be indirectly brought within FRET proximity by virtue of their binding to other molecules. This could occur if multiple copies of SQSTM1 bind to ubiquitinated substrates and/or other cargo ligands, a process that may be artificially enhanced due to the presence of endogenous SQSTM1 under the conditions of our experiments. Another possible explanation is that SQSTM1 may oligomerize by mechanisms independent of either the K7 and D69 residues and/or the PB1 domain. In support of this possibility, the SQSTM1 UBA domain appears to have a propensity for dimerization *in vitro*,⁵⁵ full-length SQSTM1 undergoes UBA domain-mediated dimerization⁵⁶ and recent results also now suggest that both a delta PB1 domain mutant of SQSTM1 and a K7A D69A mutant of SQSTM1 form trimers via an unknown mechanism.³⁴ In future work, it will be important to completely eliminate the presence of endogenous SQSTM1 to be able to more cleanly differentiate between these possibilities.

Our measurements also readily detected the presence of soluble LC3-SQSTM1 complexes in living cells. Interestingly, we found that the hydrodynamic radius of Venus-LC3, as inferred from its D , became larger upon coexpression with Cerulean-SQSTM1. D for Venus-LC3 in the presence of Cerulean-SQSTM1 ($\sim 8 \mu\text{m}^2/\text{s}$) was, however, still faster than that of Venus-SQSTM1 alone ($\sim 4 \mu\text{m}^2/\text{s}$). Two possible models could explain these findings: (i) only a fraction of Venus-LC3 may be bound to Cerulean-SQSTM1 under these conditions; or (ii) SQSTM1-associated complexes and LC3-associated complexes may remodel upon interacting with one another. It is difficult to resolve multiple classes of diffusing species by FRAP, but other approaches such as fluorescence correlation spectroscopy and fluorescence polarization and fluctuation analysis^{12,57} could be used to test this hypothesis further in future studies. Interestingly, recent evidence suggests that helical filaments formed by SQSTM1 homo-oligomerization are disassembled in response to binding to K63-linked octa-ubiquitin, but not mono- or di-ubiquitin *in vitro*.³⁶ *In vitro*, however, the filaments remain intact upon LC3 binding.³⁶ Whether this is also the case in live cells remains an open question.

Interestingly, we also found that LC3 retains the ability to bind to SQSTM1 even when the PB1 domain of SQSTM1 is disrupted. This implies that SQSTM1 homo-oligomerization is not required for LC3 to bind to SQSTM1, a result in agreement with a very recent study.³⁴ Indeed, forms of SQSTM1 that are unable to oligomerize were found to interact even more strongly with soluble LC3 than does wild-type SQSTM1.³⁴ As discussed above, however, the PB1 domain mutant of SQSTM1 and SQSTM1 isoform 2 themselves appeared to be contained within much larger complexes that contained multiple copies of SQSTM1 in FRET proximity. Thus, it seems likely that soluble LC3 is binding to a large complex that contains multiple copies of SQSTM1 in close proximity to one another under all of these conditions, rather than truly monomeric forms of SQSTM1.

As negative controls for our studies, we examined the interaction of a F52A L53A mutant of LC3 with SQSTM1, as well as a LIR mutant of SQSTM1 with LC3. LC3's F52 and L53 residues are critical for LC3's interaction with SQSTM1, and they also regulate interactions with other binding partners.^{16,25}

Furthermore, the F52 and L53 residues are in principle close enough to interact with residues K49 and K51—sites of acetylation that were recently shown to regulate LC3's binding to DOR, an interaction that enables LC3 to be carried out of the nucleus in response to amino acid starvation.¹⁵ In the context of the SQSTM1 overexpression experiments presented in this paper, the primary effect of the LC3^{F52A,L53A} mutations under steady state conditions is to mitigate a direct interaction with SQSTM1, and thus disrupt any subsequent changes in LC3's N/C ratio. Indeed, the LC3^{F52A,L53A} mutant's ability to interact with overexpressed SQSTM1 was profoundly inhibited by all the measures reported here. In contrast, the LIR mutant of SQSTM1 (D337-339A) demonstrated some ability to interact with overexpressed LC3, albeit less than wild-type SQSTM1. The simplest explanation for this finding is that we examined complexes containing overexpressed SQSTM1 and LC3 in the presence of the endogenous forms of the proteins. For the case of LC3, the levels of overexpression were 50-fold or higher, and thus the behavior of endogenous LC3 likely contributed minimally to the properties of the complexes. However, tagged SQSTM1 was present at only ~6 times that of the endogenous protein, and thus endogenous SQSTM1's contributions could potentially affect the interpretation of some of our results. This is particularly the case for the LIR mutant of SQSTM1, which contains an intact PB1 domain and is capable of forming complexes with endogenous SQSTM1, which contains a functional LIR. The formation of such mixed complexes could potentially explain why FRET was observed between Venus-LC3 and Cerulean-SQSTM1^{D337-339A}.

In the current study, we utilized 3 sensitive and robust complementary assays (FRAP, FRET, and N/C ratio measurements) to monitor the interaction of fluorescent protein chimeras of SQSTM1 and LC3 in living cells using fluorescence microscopy. Strikingly, we found that a simple assay that quantifies changes in the nucleocytoplasmic distribution of Venus-LC3 in the presence of SQSTM1 is a sensitive reporter of complex formation. This assay takes advantage of the fact that transiently overexpressed LC3 is found in both the cytoplasm and nucleoplasm, LC3 lacks active nucleocytoplasmic transport signals, and normally undergoes slow transport between the nucleus and cytoplasm.¹¹ Many LC3 interacting proteins, however, have intrinsic NES and NLS signals that regulate their nucleocytoplasmic distribution. SQSTM1 has both NLS and NES signals, but its NES signal dominates its steady-state localization, causing it to be enriched in the cytoplasm.³⁵ Overexpression of SQSTM1 drives complex formation between LC3 and SQSTM1, and under these conditions, the localization of LC3 appears to be dominated by SQSTM1's XPO1-mediated NES. As a result, co-expression of Cerulean-SQSTM1 with Venus-LC3 leads to a dramatic shift in the subcellular distribution of Venus-LC3 out of the nucleus. Even SQSTM1 PB1 domain mutants that do not form puncta are capable of modulating LC3's nucleocytoplasmic distribution. This type of regulation of LC3's localization by interacting proteins that contain an NES may be quite common, as it has also been observed in the context of the nuclear protein DOR recruiting LC3 to the cytoplasm in response to autophagy activation.^{15,58,59} Remarkably, we found that this assay was highly sensitive to the presence of overexpressed SQSTM1, as well as mutations in LC3 that disrupt SQSTM1 binding. This is important because this assay is extremely straightforward, can be used to

study soluble proteins, and also has the potential to be easily converted to a high-throughput format. It thus can be used to complement existing imaging-based approaches that focus on colocalization of proteins on specific subcellular structures, such as phagophores, autophagosomes or SQSTM1-induced puncta.

In conclusion, our results suggest a model in which soluble SQSTM1 associates with very large, slowly diffusing complexes in the cytoplasm, independent of puncta, under steady-state conditions. These complexes likely consist of multiple copies of SQSTM1 bound to polyubiquitinated cargo and/or other known SQSTM1-binding proteins, perhaps in the form of large interconnected networks. Importantly, they are detectable even under conditions where SQSTM1 does not associate with large insoluble puncta. Thus, our current results suggest the mechanisms by which SQSTM1 associates with the puncta and with the soluble complexes described here are distinct. In addition, we show that soluble SQSTM1 binds to LC3 to form slowly diffusing complexes independent of puncta. Future studies will be required to identify additional components of these complexes and to determine how their assembly and disassembly is regulated in response to autophagy-inducing stimuli.

Materials and methods

Cells and constructs

Constructs used in this study are summarized in Figure S1. Venus-LC3 and Venus-LC3 mutants were previously described.¹² Mouse wild-type SQSTM1, SQSTM1^{K7A,D69A}, and SQSTM1^{D337-339A} constructs were purchased from Addgene (38277, 38281, and 38280, deposited by Noboru Mizushima). Venus- and Cerulean-SQSTM1 vectors were constructed by first amplifying the SQSTM1 cDNA using PCR with the following forward and reverse primers:

Forward – 5'-GAGAGAAGATCTATGGCGTCGTTCCACGGTGAAG-3'

Reverse – 5'-CTGAATGTCGACTGTGGAGGGTGCTT-3'

We then inserted the SQSTM1 cDNA into Venus-C1 or Cerulean-C1 vectors (Addgene, 27794 and 27796; deposited by Steven Vogel) by double-restriction digestion with enzymes, BglII (NEB R0144S) and SalI (NEB R0138S). Venus-SQSTM1 and Cerulean-SQSTM1^{iso2} (human) were constructed by BglII and EcoRI double restriction digestion of Venus-C1, Cerulean-C1, and DsRed-SQSTM1 vectors (Addgene, 28024; deposited by Qing Zhong). An NES-Venus-LC3 construct was generated by PCR with forward primer 5'-AATTAACCGGTATGCTACACCGCTTGAGAGACTTACTCTTGTGAGCAAGGGC-3' and reverse primer 5'-TTAATTGTACAGCTCGTCCATGCCGAGAGTGATCCCGG-3'. Subsequently, the amplified DNA was inserted into the Venus-C1 vector by digestion with BsrGI and AgeI. All constructs were verified by sequencing.

HeLa cells (American Type Culture Collection; CCL-2) were cultured in Dulbecco's modified Eagle's medium containing 10% fetal bovine serum (Life Technologies; 10437028), 1% Pen-Strep, and phenol red at 37°C, 5% CO₂. For live-cell imaging experiments, on the day prior to transfection, HeLa cells were plated in MatTek 35-mm No. 1.5 glass bottom culture dishes (Ashland, P35G-1.5-10-C). On the following day, the cells (50% to 80% confluent monolayer) were transfected with described mammalian expression constructs using FuGENE6 transfection reagent

(Promega Corp., E2691) according to the manufacturer's recommended protocol. Cells were rinsed and imaged in phenol red free Dulbecco's modified Eagle's medium supplemented with 10% fetal bovine serum, 1% Pen-Strep, and 25 mM HEPES, pH 7.6. For some experiments, nuclei were labeled for 5 min with 5 mM DRAQ5 (Cell Signaling Technology, 4084L) prior to imaging in order to facilitate automated image analysis. In order to inhibit XPO1-mediated active nuclear export, leptomycin B (Sigma, L2913) at 40 nM, or as a control, an equivalent volume of 70% methanol (vehicle) were added to each dish and cells were incubated for 2 h at 37°C prior to labeling with DRAQ5 and imaging in the continued presence of LMB.

Confocal microscopy

Confocal microscopy was performed using a Zeiss LSM 510 laser scanning confocal microscope with a Zeiss 40X 1.3 NA NeoFluar oil immersion objective and an Argon/2 30 mW laser (458, 488, 514 nm) and HeNe2 laser (633 nm) (Carl Zeiss Microscopy, Inc; Thornwood, NY) as previously described.¹² The cells were maintained at 37°C using an objective heater and stage heater.

Quantification of nucleocytoplasmic ratios

Quantification of the nucleocytoplasmic ratio of soluble LC3 was performed using a custom MATLAB algorithm (freely available at <https://github.com/kraftlj/LocalizeLC3>). In our approach, confocal images were acquired for the CFP, YFP, and far red channels, enabling segmentation using binary masks for: (i) the cell and nucleus using a manually defined threshold intensity in either the YFP or the far red channel, respectively; (ii) the puncta by first subtracting the uneven diffuse cellular signal using a median filtering approach; (iii) the cytoplasm by subtracting the nucleus and puncta masks from the cell mask; and (iv) the nucleoplasm by subtracting the puncta mask from the nucleus mask. We defined the nucleocytoplasmic ratio as the mean intensity of the puncta-independent nucleus region divided by the mean intensity of the puncta-independent cytoplasm region.

Quantification of overexpression levels of tagged constructs

To assess the degree of overexpression of the tagged-SQSTM1 and LC3 constructs in HeLa cells, MatTek dishes were seeded with HeLa cells, and transfected with Venus, Venus-LC3 or mutants, Venus-SQSTM1 or mutants, or Venus-SQSTM1^{iso2} using FuGENE as described above. The next day, the cells were labeled with DRAQ5 and imaged live. Images were collected for 5-8 fields of cells per MatTek dish, and the percentage of transfected cells quantified from the images automatically (script available upon request). The experiment was repeated twice.

After imaging, the cells in each dish were lysed using cell lysis buffer (Sigma, C3228) in the presence of protease and phosphatase inhibitor cocktail (Roche, 04693159001 and 04906845001). Cell lysates were freeze-thawed twice before centrifuging at 12,000 g for 10 min at 4°C to pellet cellular debris. The total concentration of protein in each supernatant sample was quantified using BCA (Pierce, 23225), and equal amounts of protein from each sample

were loaded and separated by SDS-PAGE using NuPAGE Novex 4-12% Bis-Tris-MOPS SDS gels (Invitrogen, NP0323BOX), as per the manufacturer's directions. Western blotting was performed in a standard fashion, with 1:5000 rabbit polyclonal anti-MAP1LC3B (Novus, NB100-2220), 1:2000 guinea pig polyclonal anti-SQSTM1 (Progen, GP62), 1:2000 mouse monoclonal anti-SQSTM1 (BD, 610832), 1:10000 goat anti-rabbit IR dye-800CW, donkey anti-guinea pig IR dye 680 LT and donkey anti-mouse IR dye 800 CW (LI-COR, 926-32211, 926-68030 and 926-32212, respectively). The blots were imaged using an Odyssey infrared imaging system (LI-COR Biosciences), and quantified using ImageJ 1.48v (<http://imagej.nih.gov/ij/>).

The percent overexpression was defined as the average intensity of bands positive for Venus-LC3 (detected by LC3 antibody) or Venus-SQSTM1 (detected by anti-SQSTM1, Progen antibody) or Venus-SQSTM1^{iso2} (detected by anti-SQSTM1, BD antibody) (corrected using the transfection efficiency that was obtained from confocal images as described above) divided by the intensity of the corresponding endogenous protein bands.

Acceptor photobleaching FRET

For acceptor photobleaching experiments, the cells were cotransfected with donor (Cerulean) and acceptor (Venus) tagged constructs. Acceptor photobleaching FRET measurements were performed by imaging the donor using a 458-nm laser and the acceptor using a 514-nm laser as previously described.¹⁴ The imaging laser power was set such that unintentional photobleaching during image acquisition was minimal. Images in the donor (D_{pre} and D_{post}) and acceptor (A_{pre} and A_{post}) channels were collected both before and after photobleaching the acceptor. In order to photobleach the acceptor, the entire cell was exposed to the 514-nm laser set to a nominal power of 30 mW for several iterations. Under these conditions, the acceptor was photobleached to <5% of its pre-bleach intensity.

Acceptor photobleaching FRET data were analyzed using an automated approach, and our MATLAB scripts for quantifying FRET are available online at <https://github.com/kraftlj/abFRET>. To define the relevant regions of the images for analysis, binary masks were created for the cell and the background using a manually defined threshold intensity in the acceptor channel, while masks were defined for the puncta by first subtracting the uneven diffuse cellular signal using a median filtering approach. Lateral movement of the donor images before and after photobleaching was corrected by cross-correlation. The averaged energy transfer efficiency (E) for the background-subtracted cell (devoid of puncta) or for puncta was calculated according to:

$$\%E = ([D_{post} - D_{pre}] / D_{post}) \times 100 \quad (1)$$

where (D_{pre}) corresponds to the background-subtracted fluorescence intensity of the donor prior to bleaching the acceptors and (D_{post}) represents the background subtracted donor intensity after photobleaching the acceptor.

FRAP

In order to quantify diffusion in cells, FRAP measurements were performed as recently described.¹² In brief, a rectangular imaging region of interest (ROI) was used for increased temporal resolution, and a small circular 1- μm radius bleach ROI, r_m , centered in an area of the cytoplasm devoid of puncta was used for bleaching. The proteins analyzed in this study rapidly diffuse, and thus the frame rate was set to the maximum speed of approximately 40 frames per sec. The photobleaching was carried out using the 514-nm laser line at the full nominal power of 30 mW, while the imaging was carried out using a greatly attenuated nominal laser power of 60 μW with the goal of minimizing unintentional photobleaching over the observational period.

The FRAP data were analyzed using FRAP-Toolbox—a freely available software for the analysis of FRAP data, written in house, and available online at <http://www.fraptoolbox.com>. In particular, the single component diffusion model fit all of the FRAP curves in this study well. For this model, the initial conditions to solve the diffusion equation were found by fitting the radial distribution of fluorescence from the post-bleach profile to the following analytical approximation:

$$I(x; t = 0) = I_0 \exp\left(-K \exp\left[-\frac{2x^2}{r_e^2}\right]\right) \quad (2)$$

where I_0 is 1 for normalized FRAP data, K is the bleach depth, x is the radial distance from the center of the bleach ROI, and r_e is the effective bleach radius. The average intensity inside the bleach ROI over time, the FRAP curve $I(t)$ was fit to a series representation of the closed form analytical FRAP equation:

$$I(t) = I_0 \left(\sum_{m=0}^{m=200} \frac{-K^m r_e^2}{m! [r_e^2 + m(8Dt + r_n^2)]} \right) Mf + (1 - Mf)I(0) \quad (3)$$

This is a generalized form of the conventional Axelrod equation that is applicable to data obtained on a confocal microscope. The parameters K and r_e account for diffusion that occurs before acquisition of the post-bleach image. This model was validated in a previous publication, and there it was shown that without these corrections, D measured by confocal FRAP can be dramatically underestimated.⁶⁰

Statistics

Values reported throughout the text are the mean \pm 95% confidence intervals. Statistical comparisons were made using a Bonferonni corrected t test, in order to control the overall type-I error rate at 0.05 where multiple comparisons were made. For example, if 5 pairs of comparisons were made, the p-value threshold was set to 0.01.

Abbreviations

ATG	autophagy related
D	diffusion coefficient

E	energy transfer efficiency
FPFA	fluorescence polarization and fluctuation analysis
FRAP	fluorescence recovery after photobleaching
FRET	Förster resonance energy transfer
LC3-I	soluble microtubule-associated protein 1 light chain 3
LC3-II	lipid-modified microtubule-associated protein 1 light chain 3
LIR	LC3-interacting region
LMB	leptomycin B
MAP1LC3B/LC3B	microtubule associated protein 1 light chain 3 β
MTORC1	mechanistic target of rapamycin (serine/threonine kinase) complex 1
N/C	nucleocytoplasmic
NES	nuclear export signal
NLS	nuclear localization signal
PB1	phox and bem1 domain
ROI	region of interest
SQSTM1	sequestosome 1
SQSTM1 ^{iso2}	physiologically present less abundant isoform 2 of SQSTM1 lacking PB1 domain
UPS	ubiquitin-proteasome system

Disclosure of potential conflicts of interest

No potential conflicts of interest were disclosed.

Acknowledgments

We thank Kimberly Drake for her expert technical assistance.

Funding

This work was funded by grant NSF/DMS 0970008 from the National Science Foundation, and utilized the core(s) of the Vanderbilt Diabetes Research and Training Center funded by grant DK020593 from the National Institute of Diabetes and Digestive and Kidney Disease. The funding sources had no role in the study design, collection, analysis or interpretation of data, writing the report, or the decision to submit the paper for publication.

References

- [1] Yang Z, Klionsky DJ. Eaten alive: a history of macroautophagy. *Nat Cell Biol* 2010; 12:814-22; PMID:20811353; <http://dx.doi.org/10.1038/ncb0910-814>
- [2] Choi AM, Ryter SW, Levine B. Autophagy in human health and disease. *N Engl J Med* 2013; 368:651-62; PMID:23406030; <http://dx.doi.org/10.1056/NEJMra1205406>
- [3] Lazarou M, Sliter DA, Kane LA, Sarraf SA, Wang C, Burman JL, Sideris DP, Fogel AI, Youle RJ. The ubiquitin kinase PINK1 recruits autophagy receptors to induce mitophagy. *Nature* 2015; 524:309-14; PMID:26266977; <http://dx.doi.org/10.1038/nature14893>
- [4] Johansen T, Lamark T. Selective autophagy mediated by autophagic adapter proteins. *Autophagy* 2011; 7:279-96; PMID:21189453; <http://dx.doi.org/10.4161/auto.7.3.14487>
- [5] Kirkin V, McEwan DG, Novak I, Dikic I. A role for ubiquitin in selective autophagy. *Mol Cell* 2009; 34:259-69; PMID:19450525; <http://dx.doi.org/10.1016/j.molcel.2009.04.026>

- [6] Weidberg H, Shvets E, Elazar Z. Biogenesis and cargo selectivity of autophagosomes. *Annu Rev Biochem* 2011; 80:125-56; PMID:21548784; <http://dx.doi.org/10.1146/annurev-biochem-052709-094552>
- [7] Shpilka T, Weidberg H, Pietrokovski S, Elazar Z. Atg8: an autophagy-related ubiquitin-like protein family. *Genome Biol* 2011; 12:226; PMID:21867568; <http://dx.doi.org/10.1186/gb-2011-12-7-226>
- [8] Kabeya Y, Mizushima N, Ueno T, Yamamoto A, Kirisako T, Noda T, Kominami E, Ohsumi Y, Yoshimori T. LC3, a mammalian homologue of yeast Apg8p, is localized in autophagosome membranes after processing. *Embo J* 2000; 19:5720-8; PMID:11060023; <http://dx.doi.org/10.1093/emboj/19.21.5720>
- [9] Kabeya Y, Mizushima N, Yamamoto A, Oshitani-Okamoto S, Ohsumi Y, Yoshimori T. LC3, GABARAP and GATE16 localize to autophagosomal membrane depending on form-II formation. *J Cell Sci* 2004; 117:2805-12; PMID:15169837; <http://dx.doi.org/10.1242/jcs.01131>
- [10] Satoo K, Noda NN, Kumeta H, Fujioka Y, Mizushima N, Ohsumi Y, Inagaki F. The structure of Atg4B-LC3 complex reveals the mechanism of LC3 processing and delipidation during autophagy. *Embo J* 2009; 28:1341-50; PMID:19322194; <http://dx.doi.org/10.1038/emboj.2009.80>
- [11] Drake KR, Kang M, Kenworthy AK. Nucleocytoplasmic distribution and dynamics of the autophagosome marker EGFP-LC3. *PLoS ONE* 2010; 5:e9806; PMID:20352102; <http://dx.doi.org/10.1371/journal.pone.0009806>
- [12] Kraft LJ, Nguyen TA, Vogel SS, Kenworthy AK. Size, stoichiometry, and organization of soluble LC3-associated complexes. *Autophagy* 2014; 10:861-77; PMID:24646892; <http://dx.doi.org/10.4161/auto.28175>
- [13] Kraft LJ, Manral P, Dowler J, Kenworthy AK. Nuclear LC3 associates with slowly diffusing complexes that survey the nucleolus. *Traffic* 2016; PMID:26728248
- [14] Kraft LJ, Kenworthy AK. Imaging protein complex formation in the autophagy pathway: analysis of the interaction of LC3 and Atg4B(C74A) in live cells using Forster resonance energy transfer and fluorescence recovery after photobleaching. *J Biomed Opt* 2012; 17:011008; PMID:22352642; <http://dx.doi.org/10.1117/1.JBO.17.1.011008>
- [15] Huang R, Xu Y, Wan W, Shou X, Qian J, You Z, Liu B, Chang C, Zhou T, Lippincott-Schwartz J, et al. Deacetylation of nuclear LC3 drives autophagy initiation under starvation. *Mol Cell* 2015; 57:456-66; PMID:25601754; <http://dx.doi.org/10.1016/j.molcel.2014.12.013>
- [16] Behrends C, Sowa ME, Gygi SP, Harper JW. Network organization of the human autophagy system. *Nature* 2010; 466:68-76; PMID:20562859; <http://dx.doi.org/10.1038/nature09204>
- [17] Birgisdottir AB, Lamark T, Johansen T. The LIR motif - crucial for selective autophagy. *J Cell Sci* 2013; 126:3237-47; PMID:23908376
- [18] Bjorkoy G, Lamark T, Brech A, Outzen H, Perander M, Overvatn A, Stenmark H, Johansen T. p62/SQSTM1 forms protein aggregates degraded by autophagy and has a protective effect on huntingtin-induced cell death. *J Cell Biol* 2005; 171:603-14; PMID:16286508; <http://dx.doi.org/10.1083/jcb.200507002>
- [19] Lamark T, Kirkin V, Dikic I, Johansen T. NBR1 and p62 as cargo receptors for selective autophagy of ubiquitinated targets. *Cell Cycle* 2009; 8:1986-90; PMID:19502794; <http://dx.doi.org/10.4161/cc.8.13.8892>
- [20] Ichimura Y, Komatsu M. Selective degradation of p62 by autophagy. *Semin Immunopathol* 2010; 32:431-6; PMID:20814791; <http://dx.doi.org/10.1007/s00281-010-0220-1>
- [21] Pankiv S, Clausen TH, Lamark T, Brech A, Bruun JA, Outzen H, Overvatn A, Bjorkoy G, Johansen T. p62/SQSTM1 binds directly to Atg8/LC3 to facilitate degradation of ubiquitinated protein aggregates by autophagy. *J Biol Chem* 2007; 282:24131-45; PMID:17580304; <http://dx.doi.org/10.1074/jbc.M702824200>
- [22] Ichimura Y, Kumanoimidou T, Sou YS, Mizushima T, Ezaki J, Ueno T, Kominami E, Yamane T, Tanaka K, Komatsu M. Structural basis for sorting mechanism of p62 in selective autophagy. *J Biol Chem* 2008; 283:22847-57; PMID:18524774; <http://dx.doi.org/10.1074/jbc.M8021-82200>
- [23] Shvets E, Elazar Z. Autophagy-independent incorporation of GFP-LC3 into protein aggregates is dependent on its interaction with p62/SQSTM1. *Autophagy* 2008; 4:1054-6; PMID:18776740; <http://dx.doi.org/10.4161/auto.6823>
- [24] Komatsu M, Waguri S, Koike M, Sou YS, Ueno T, Hara T, Mizushima N, Iwata J, Ezaki J, Murata S, et al. Homeostatic levels of p62 control cytoplasmic inclusion body formation in autophagy-deficient mice. *Cell* 2007; 131:1149-63; PMID:18083104; <http://dx.doi.org/10.1016/j.cell.2007.10.035>
- [25] Shvets E, Fass E, Scherz-Shouval R, Elazar Z. The N-terminus and Phe52 residue of LC3 recruit p62/SQSTM1 into autophagosomes. *J Cell Sci* 2008; 121:2685-95; PMID:18653543; <http://dx.doi.org/10.1242/jcs.026005>
- [26] Shvets E, Abada A, Weidberg H, Elazar Z. Dissecting the involvement of LC3B and GATE-16 in p62 recruitment into autophagosomes. *Autophagy* 2011; 7:683-8; PMID:21460636; <http://dx.doi.org/10.4161/auto.7.7.15279>
- [27] Ichimura Y, Kominami E, Tanaka K, Komatsu M. Selective turnover of p62/A170/SQSTM1 by autophagy. *Autophagy* 2008; 4:1063-6; PMID:18776737; <http://dx.doi.org/10.4161/auto.6826>
- [28] Noda NN, Kumeta H, Nakatogawa H, Satoo K, Adachi W, Ishii J, Fujioka Y, Ohsumi Y, Inagaki F. Structural basis of target recognition by Atg8/LC3 during selective autophagy. *Genes Cells* 2008; 13:1211-8; PMID:19021777; <http://dx.doi.org/10.1111/j.1365-2443.2008.01238.x>
- [29] Gao Z, Gammoh N, Wong PM, Erdjument-Bromage H, Tempst P, Jiang X. Processing of autophagic protein LC3 by the 20S proteasome. *Autophagy* 2010; 6:126-37; PMID:20061800; <http://dx.doi.org/10.4161/auto.6.1.10928>
- [30] Itakura E, Mizushima N. p62 Targeting to the autophagosome formation site requires self-oligomerization but not LC3 binding. *J Cell Biol* 2011; 192:17-27; PMID:21220506; <http://dx.doi.org/10.1083/jcb.2010-09067>
- [31] Lamark T, Perander M, Outzen H, Kristiansen K, Overvatn A, Michaelsen E, Bjorkoy G, Johansen T. Interaction codes within the family of mammalian Phox and Bem1p domain-containing proteins. *J Biol Chem* 2003; 278:34568-81; PMID:12813044; <http://dx.doi.org/10.1074/jbc.M303221200>
- [32] Wilson MI, Gill DJ, Perisic O, Quinn MT, Williams RL. PB1 domain-mediated heterodimerization in NADPH oxidase and signaling complexes of atypical protein kinase C with Par6 and p62. *Mol Cell* 2003; 12:39-50; PMID:12887891; [http://dx.doi.org/10.1016/S1097-2765\(03\)00246-6](http://dx.doi.org/10.1016/S1097-2765(03)00246-6)
- [33] Kirkin V, Lamark T, Sou YS, Bjorkoy G, Nunn JL, Bruun JA, Shvets E, McEwan DG, Clausen TH, Wild P, et al. A role for NBR1 in autophagosomal degradation of ubiquitinated substrates. *Mol Cell* 2009; 33:505-16; PMID:19250911; <http://dx.doi.org/10.1016/j.molcel.2009.01.020>
- [34] Wurzer B, Zaffagnini G, Fracchiolla D, Turco E, Abert C, Romanov J, Martens S. Oligomerization of p62 allows for selection of ubiquitinated cargo and isolation membrane during selective autophagy. *Elife* 2015; 4:e08941; PMID:26413874; <http://dx.doi.org/10.7554/eLife.08941.002>
- [35] Pankiv S, Lamark T, Bruun JA, Overvatn A, Bjorkoy G, Johansen T. Nucleocytoplasmic shuttling of p62/SQSTM1 and its role in recruitment of nuclear polyubiquitinated proteins to promyelocytic leukemia bodies. *J Biol Chem* 2010; 285:5941-53; PMID:20018885; <http://dx.doi.org/10.1074/jbc.M109.039925>
- [36] Ciuffa R, Lamark T, Tarafder AK, Guesdon A, Rybina S, Hagen WJ, Johansen T, Sachse C. The selective autophagy receptor p62 forms a flexible filamentous helical scaffold. *Cell Rep* 2015; 11:748-58; PMID:25921531; <http://dx.doi.org/10.1016/j.celrep.2015.03.062>
- [37] Tanida I, Yamaji T, Ueno T, Ishiura S, Kominami E, Hanada K. Consideration about negative controls for LC3 and expression vectors for four colored fluorescent protein-LC3 negative controls. *Autophagy* 2008; 4:131-4; PMID:18000393; <http://dx.doi.org/10.4161/auto.5233>
- [38] Vogel SS, Thaler C, Koushik SV. Fanciful FRET. *Sci STKE* 2006; 2006:re2; PMID:16622184
- [39] Day RN, Davidson MW. Fluorescent proteins for FRET microscopy: monitoring protein interactions in living cells. *Bioessays* 2012; 34:341-50; PMID:22396229; <http://dx.doi.org/10.1002/bies.201100098>
- [40] Sun Y, Wallrabe H, Seo SA, Periasamy A. FRET microscopy in 2010: the legacy of Theodor Forster on the 100th anniversary of his birth. *Chemphyschem* 2011; 12:462-74; PMID:21344587; <http://dx.doi.org/10.1002/cphc.201000664>
- [41] Grecco HE, Verveer PJ. FRET in Cell Biology: Still Shining in the Age of Super-Resolution? *Chemphyschem* 2010; 12:484-90; PMID:21344589; <http://dx.doi.org/10.1002/cphc.201000795>

- [42] Kenworthy AK. Imaging protein-protein interactions using fluorescence resonance energy transfer microscopy. *Methods: A Companion to Methods in Enzymology* 2001; 24:289-96; <http://dx.doi.org/10.1006/meth.2001.1189>
- [43] Kenworthy AK. Photobleaching FRET Microscopy. In: Periasamy A, Day RN, eds. *Molecular Imaging: FRET Microscopy and Spectroscopy*; Oxford University Press, 2005
- [44] Wang L, Chen M, Yang J, Zhang Z. LC3 fluorescent puncta in autophagosomes or in protein aggregates can be distinguished by FRAP analysis in living cells. *Autophagy* 2013; 9:756-69; PMID: 23482084; <http://dx.doi.org/10.4161/auto.23814>
- [45] Karpova T, McNally JG. Detecting protein-protein interactions with CFP-YFP FRET by acceptor photobleaching. *Curr Protoc Cytom* 2006; Chapter 12:Unit12 7; PMID:18770833
- [46] Verveer PJ, Rocks O, Harpur AG, Bastiaens PI. Measuring FRET by acceptor photobleaching. *CSH Protoc* 2006; pii: pdb.ip15; PMID: 22485973; <http://dx.doi.org/10.1101/pdb.ip15>
- [47] Van Munster EB, Kremers GJ, Adjobo-Hermans MJ, Gadella TW, Jr. Fluorescence resonance energy transfer (FRET) measurement by gradual acceptor photobleaching. *J Microsc* 2005; 218:253-62; PMID: 15958019; <http://dx.doi.org/10.1111/j.1365-2818.2005.01483.x>
- [48] Rogov V, Dotsch V, Johansen T, Kirkin V. Interactions between Autophagy Receptors and Ubiquitin-like Proteins Form the Molecular Basis for Selective Autophagy. *Mol Cell* 2014; 53:167-78; PMID:24462201; <http://dx.doi.org/10.1016/j.molcel.2013.12.014>
- [49] Wang L, Cano M, Handa JT. p62 provides dual cytoprotection against oxidative stress in the retinal pigment epithelium. *Biochim Biophys Acta* 2014; 1843:1248-58; PMID:24667411; <http://dx.doi.org/10.1016/j.bbamcr.2014.03.016>
- [50] De La Torre JG, Martinez MCL, Tirado MM. Dimensions of short, rodlike macromolecules from translational and rotational diffusion coefficients. Study of the gramicidin dimer. *Biopolymers* 1984; 23:611-5; <http://dx.doi.org/10.1002/bip.360230402>
- [51] Seibenhener ML, Geetha T, Wooten MW. Sequestosome 1/p62—more than just a scaffold. *FEBS Lett* 2007; 581:175-9; PMID:17188686; <http://dx.doi.org/10.1016/j.febslet.2006.12.027>
- [52] Duran A, Amanchy R, Linares JF, Joshi J, Abu-Baker S, Porollo A, Hansen M, Moscat J, Diaz-Meco MT. p62 is a key regulator of nutrient sensing in the mTORC1 pathway. *Mol Cell* 2011; 44:134-46; PMID:21981924; <http://dx.doi.org/10.1016/j.molcel.2011.06.038>
- [53] Groll M, Ditzel L, Lowe J, Stock D, Bochtler M, Bartunik HD, Huber R. Structure of 20S proteasome from yeast at 2.4 Å resolution. *Nature* 1997; 386:463-71; PMID:9087403; <http://dx.doi.org/10.1038/386463a0>
- [54] Seibenhener ML, Babu JR, Geetha T, Wong HC, Krishna NR, Wooten MW. Sequestosome 1/p62 is a polyubiquitin chain binding protein involved in ubiquitin proteasome degradation. *Mol Cell Biol* 2004; 24:8055-68; PMID:15340068; <http://dx.doi.org/10.1128/MCB.24.18.8055-8068.2004>
- [55] Long J, Garner TP, Pandya MJ, Craven CJ, Chen P, Shaw B, Williamson MP, Layfield R, Searle MS. Dimerisation of the UBA domain of p62 inhibits ubiquitin binding and regulates NF- κ B signalling. *J Mol Biol* 2010; 396:178-94; PMID:19931284; <http://dx.doi.org/10.1016/j.jmb.2009.11.032>
- [56] Isogai S, Morimoto D, Arita K, Unzai S, Tenno T, Hasegawa J, Sou YS, Komatsu M, Tanaka K, Shirakawa M, et al. Crystal structure of the ubiquitin-associated (UBA) domain of p62 and its interaction with ubiquitin. *J Biol Chem* 2011; 286:31864-74; PMID:21715324; <http://dx.doi.org/10.1074/jbc.M111.259630>
- [57] Nguyen TA, Sarkar P, Veetil JV, Koushik SV, Vogel SS. Fluorescence polarization and fluctuation analysis monitors subunit proximity, stoichiometry, and protein complex hydrodynamics. *PLoS ONE* 2012; 7:e38209; PMID:22666486; <http://dx.doi.org/10.1371/journal.pone.0038209>
- [58] Nowak J, Archange C, Tardivel-Lacombe J, Pontarotti P, Pebusque MJ, Vaccaro MI, Velasco G, Dagorn JC, Iovanna JL. The TP53INP2 protein is required for autophagy in mammalian cells. *Mol Biol Cell* 2009; 20:870-81; PMID:19056683; <http://dx.doi.org/10.1091/mbc.E08-07-0671>
- [59] Sancho A, Duran J, Garcia-Espana A, Mauvezin C, Alemu EA, Lamark T, Macias MJ, DeSalle R, Royo M, Sala D, et al. DOR/Tp53inp2 and Tp53inp1 constitute a metazoan gene family encoding dual regulators of autophagy and transcription. *PLoS One* 2012; 7:e34034; PMID:22470510; <http://dx.doi.org/10.1371/journal.pone.0034034>
- [60] Kang M, Day CA, Drake K, Kenworthy AK, DiBenedetto E. A generalization of theory for two-dimensional fluorescence recovery after photobleaching applicable to confocal laser scanning microscopes. *Biophys J* 2009; 97:1501-11; PMID:19720039; <http://dx.doi.org/10.1016/j.bpj.2009.06.017>